AAPS PharmSciTech (2025) 26:224
https://doi.org/10.1208/s12249-025-03215-3

RESEARCH ARTICLE

3D-printed Gabapentin-loaded Implants for Sustained Release: Leveraging 3D Printing and Hot Melt Extrusion (HME) for Customizable Drug Delivery

Baher A. Daihom[1,2,3] · **Hala M. Abdelhakk**[1,4] · **Mohammed Maniruzzaman**[1,5]

Received: 25 March 2025 / Accepted: 7 August 2025

Abstract

Pediatric neuropathy poses significant challenges in pain management due to the limited availability of approved pharmacological options. Gabapentin, commonly used for neuropathic pain, offers therapeutic potential but necessitates careful dosing due to its variable bioavailability. This study investigates the integration of Hot Melt Extrusion and Fused Deposition Modeling in the development of polycaprolactone-based implants for sustained release of Gabapentin. A preliminary screening using Vacuum Compression Molding optimized formulations for Hot Melt Extrusion, enhancing material efficiency and process streamlining. Filaments with a diameter of 1.75 mm were successfully extruded and used for 3D printing of Gabapentin implants. Several tests were undertaken to characterize the prepared filaments and implants. Energy-Dispersive X-ray spectroscopy confirmed the uniform distribution of Gabapentin within the implant matrix. Solid-state characterization techniques were employed to assess the compatibility of implant components and to verify the solid-state of Gabapentin within the implant structure. *In vitro* drug release studies were conducted. Filaments with varying drug loadings were examined, revealing that a 20% w/w drug loading achieved an optimal balance between rapid and sustained release. Additionally, implants with different infill densities were analyzed, demonstrating that varying infill densities allow control over the amount and percentage of drug released. The 100% infill density resulted in the most sustained release effect, achieving approximately 40% drug release by day 28. These findings underscore the feasibility of 3D printing for producing personalized implants, emphasizing the potential for tailored drug release profiles to meet specific needs of pediatric patients.

Keywords 3D printing · Gabapentin · Hot melt extrusion · Implant · Vacuum compression modeling

Introduction

Pediatric neuropathy is a condition present in children, where there is peripheral nerve malfunction. These nerves play a very significant role in transmitting signals between the central nervous system and the rest of the body [1]. Effects of neuropathy can be entirely different according to the sensory, motor, or autonomic nerves involved and hence lead to a highly varied set of symptoms [2]. Pediatric neuropathic pain is very challenging for treatment in many ways, as there are few medications approved for this condition [3, 4]. When determining appropriate dosage adjustments, the child's age, weight, and developmental stage must be carefully considered [5].

Gabapentin, a freely water-soluble medication [6], has shown effectiveness as an adjunctive treatment for partial epileptic seizures [7]. Additionally, it is widely used off-label for the management of neuropathic pain [8]. In pediatric

Baher A. Daihom and Hala M. Abdelhakk contributed equally to this work.

✉ Mohammed Maniruzzaman
mmaniruz@olemiss.edu

1 Division of Molecular Pharmaceutics and Drug Delivery, College of Pharmacy, The University of Texas at Austin, Austin, TX 78712, USA

2 Department of Pharmaceutics and Industrial Pharmacy, Cairo University, Kasr El-Aini St, Cairo 11562, Egypt

3 College of Pharmacy, American University in Iraq-Baghdad, Baghdad, Iraq

4 Department of Industrial Pharmacy, Faculty of Pharmacy, Assiut University, Assiut 71526, Egypt

5 Pharmaceutical Engineering and 3D Printing (PharmE3D) Labs, Department of Pharmaceutics and Drug Delivery, School of Pharmacy, The University of Mississippi, University, MS 38677, USA

Published online: 03 September 2025

patients, Gabapentin has emerged as a valuable option for treating neuropathic, pre-and post-operative pain [9]. It works by modulating the release of specific neurotransmitters involved in pain signaling, leading to relief from neuropathic pain [10]. Numerous studies and clinical trials have demonstrated positive results with Gabapentin use in pediatric patients. It has been found to provide pain relief in burn survivors, and it prevents postoperative pain [11, 12]. Based on American Pain Society, Gabapentin should be included in pediatric neuropathic pain condition, especially when other relievers render a sedation effect. The recommended dose is an initial of 2 mg/kg/day, and the average dose ranges from 8 to 35 mg/kg/day in divided doses a day [13, 14]. Having a structural similarity to natural amino acids, such as L-leucine, Gabapentin crosses the small intestine through the active, saturable L-amino acid transport mechanism. This transport mechanism has been identified as a major determinant of the dose-dependent bioavailability of Gabapentin. In this case, it has been determined that the bioavailability of Gabapentin is inversely proportional to dosing. That is, the higher the dose, the lower the bioavailability of Gabapentin. For example, while at doses as low as 900 mg/day, its bioavailability is around 60%, the bioavailability at a higher dose of 4800 mg/day is significantly reduced to about 27% [11, 15]. There were also reports that repeated administration of Gabapentin leads to oscillations in plasma levels which, in turn, causes impairment in memory in mice [16, 17].

Additive manufacturing, widely called 3D printing, is an additive process of building an object layer by layer, using thermoplastic polymers [18]. The relevance of 3D printing technology in formulating long-acting medicinal implants lies in their capability to customize personalized implants with specified designs in their constituents according to a patient's preference [19–21]. 3D printing enables customization, incorporating multiple medications, and controlling drug release kinetics [22–24]. Fused Deposition Modeling (FDM) is one such commonly used form of 3D printing technology where a melted polymer is deposited through a heated nozzle into the desired object shape. The extrusion nozzle melts the polymer, which is deposited with precision on the build plate and allowed to solidify. This layering procedure allows for deposition of the softened polymer, with the softened polymer solidifying before adding a new layer to build up a 3D structure [25, 26]. This comes with several distinct advantages, including ease of operation, low-cost manufacturing, and the ability to create intricate structures without using any form of solvent [20, 27].

A drug-loaded polymer filament can be manufactured using Hot Melt Extrusion technology [28, 29]. HME, a continuous manufacturing technique, enables the uniform incorporation of active pharmaceutical ingredients (APIs) into a polymer matrix, ensuring precise dosage control and enhanced drug release profiles [30]. During the Hot Melt Extrusion process, the magnitude of material loss is substantial, characterized by a significant proportion of the material being dissipated during the startup phase or retained within the non-operational region of the extrude [31]. Vacuum Compression Modeling serves as a valuable preliminary technique to be employed before Hot Melt Extrusion, functioning as a small-scale screening tool that offers advantages such as minimizing material consumption and time savings. By implementing Vacuum Compression Modeling in the initial stages, material usage can be optimized, and the total processing time can be considerably shortened. This approach aids in efficiently evaluating the feasibility and performance of various formulations, enabling researchers to make informed decisions and streamline the subsequent Hot Melt Extrusion process [31, 32]. Polycaprolactone is among the most widely used polymers in the Hot Melt Extrusion process. It is biocompatible, biodegradable, not soluble in water, and has a relatively low melting point, between approximately 50 and 60°C [33]. Existing literature has identified PCL as a viable polymer carrier for 3D printing facilitated by FDM technology [34, 35].

Pediatric implants have shown efficacy in treating various medical conditions in children. One notable example is the histrelin implant, used to treat central precocious puberty (CPP). This subcutaneous implant, marketed as Supprelin LA, releases histrelin acetate, a GnRH agonist, over 12 months, effectively delaying early puberty. The minimally invasive procedure for implant insertion, typically performed under local anesthesia, underscores the feasibility and safety of such interventions in pediatric patients. The histrelin implant helps children develop in line with their age, showing how pediatric implants can improve health and quality of life [36]. Our goal is to develop PCL implants for the localized delivery of Gabapentin. This aims to overcome the bioavailability challenges associated with oral administration while reducing the need for high doses and frequent dosing. Additionally, the implants will help maintain stable plasma levels of Gabapentin, minimizing side effects.

Materials

Gabapentin (GABA) was obtained from TCI America (Tokyo Chemical Industry Co., Portland, Oregon, USA). Polycaprolactone (PCL) MW 50000 was provided by Polysciences, Inc. (Warrington, PA, USA). Polyethylene glycol (PEG) 3350 and HPLC grade acetonitrile were provided from Sigma-Aldrich Inc (St. Louis, Missouri, USA). KH_2PO_4, KOH, and all other chemicals are of analytical grades.

Methods

Chromatographic Conditions for Determination of Gabapentin

The quantification of the samples was done using a reverse-phase high-performance liquid chromatography (RP-HPLC) method (Thermo Fisher Vanquish HPLC system, Thermo Fisher, Waltham, MA, USA) equipped with a C-18 column of dimensions L × I.D. = 250 × 4.6 mm and a particle size of 5 µm (Discovery® C–18 HPLC column, Supelco™, Millipore Sigma, MA, USA). The mobile phase consisted of a buffer mixture (1.2 g KH_2PO_4 in one-liter water, pH adjusted to 6.9 with KOH) and acetonitrile, with a ratio of 90:10 (v/v) for the aqueous and organic phases, respectively. The elution was carried out at a flow rate of 1 ml/min, with a sample injection volume of 20 µL. The signals from the samples were detected using a UV–Vis spectrophotometer detector (ThermoFisher Vanquish HPLC system, Waltham, MA, USA) at λ = 200 nm [37].

Vacuum Compression Modeling (VCM)

Vacuum Compression Modeling (VCM) is a crucial preliminary tool for optimizing formulations before proceeding with Hot Melt Extrusion. It is integral to ensuring that the formulations are viable and effective before proceeding to more advanced stages of development.

Discs (25 mm diameter) were created using the Melt-Prep® VCM technique. Pre-weighed mixtures were added to molds with separation foil, heated to 80 °C for 5 min, then cooled to room temperature using compressed air. The discs were then manually removed for analysis [31, 38]. The specific compositions of various formulations can be found in (Table I).

Hot Melt Extrusion (HME)

Different formulations (Table I) were created. Pre-weighed mixtures were extruded through a Leistritz ZSE 12 HP-PH 12 mm twin-screw corotating extruder (Leistritz Advanced Technologies Corp. in Nuremberg, Germany). This advanced extruder is equipped with eight distinct zones, each optimized for specific processing conditions. To comply with the specifications of the Fused Deposition Modeling (FDM) printer, a 1.75 mm die was employed during the extrusion procedure. The Extruder, the screw design and temperature profile used for the extrusion process are shown in Fig. 1. The screw speed was adjusted at 50 r.p.m. The produced filaments were kept at room temperature in sealed bags before printing [39, 40].

Table I Formulation Composition Details

	Gabapentin (% w/w)	PCL (% w/w)	PEG3350 (%w/w)
F1	10	80	10
F2	20	70	10
F3	30	60	10
F4	50	40	10

Fabrication of Gabapentin-loaded Implants

3D-Design of the Implant

A 3D model of the implant was created using Microsoft 3D Builder (Microsoft, Redmond, WA, USA), and subsequently exported in STL file format. The implant dimensions were set at 25 × 7 mm. The implant design is shown in Fig. 2.

3D printing of the Implant

The experimental setup utilized a MakerBot Replicator® 2X Experimental 3D Printer (MakerBot Industries, New York, USA) to fabricate the implant structure. The STL file was processed using MakerBot software, with optimized printing parameters as follows: a layer thickness of 2 mm and a linear infill pattern. The print head, with a 0.4 mm diameter, operated at 110°C and a speed of 5 mm/s, while the bed temperature was maintained at 30°C throughout the printing process. To assess the impact of infill density on implant properties, three distinct densities—25%, 50%, and 100%—were investigated.

Solid State Characterization

1. Differential Scanning Calorimetry (DSC)

The thermal behavior of the drug, excipients, physical mixture, and the crushed powder of the prepared filaments and implants was investigated using Differential Scanning Calorimetry (DSC, DSCQ20, TA Instruments, New Castle, DE, USA). Samples (5–10 mg) were weighed into DSC aluminum pans and sealed with lids. Samples were heated from 35°C to 220°C at 10°C/min with nitrogen purge gas at 50 mL/min. Data was collected using TA advantage software [41].

2. X-ray Powder Diffraction (XRPD) Studies

X-ray Powder Diffraction patterns for the drug, excipients, physical mixtures, and the crushed powder of the prepared filaments and implants were collected using a benchtop Rigaku MiniFlex 600 (Rigaku Corporation, Tokyo,

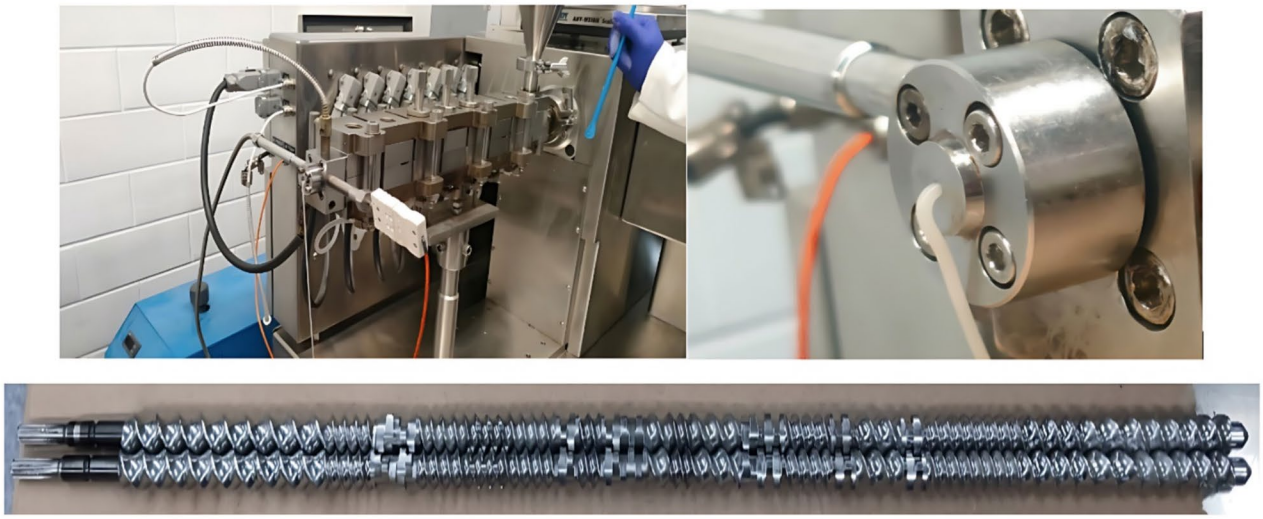

Zone	1	2	3	4	5	6	7	8	9
Temp	40	50	60	80	80	80	80	70	60

Fig. 1 The extruder, screw design, and temperature profile used in the extrusion process

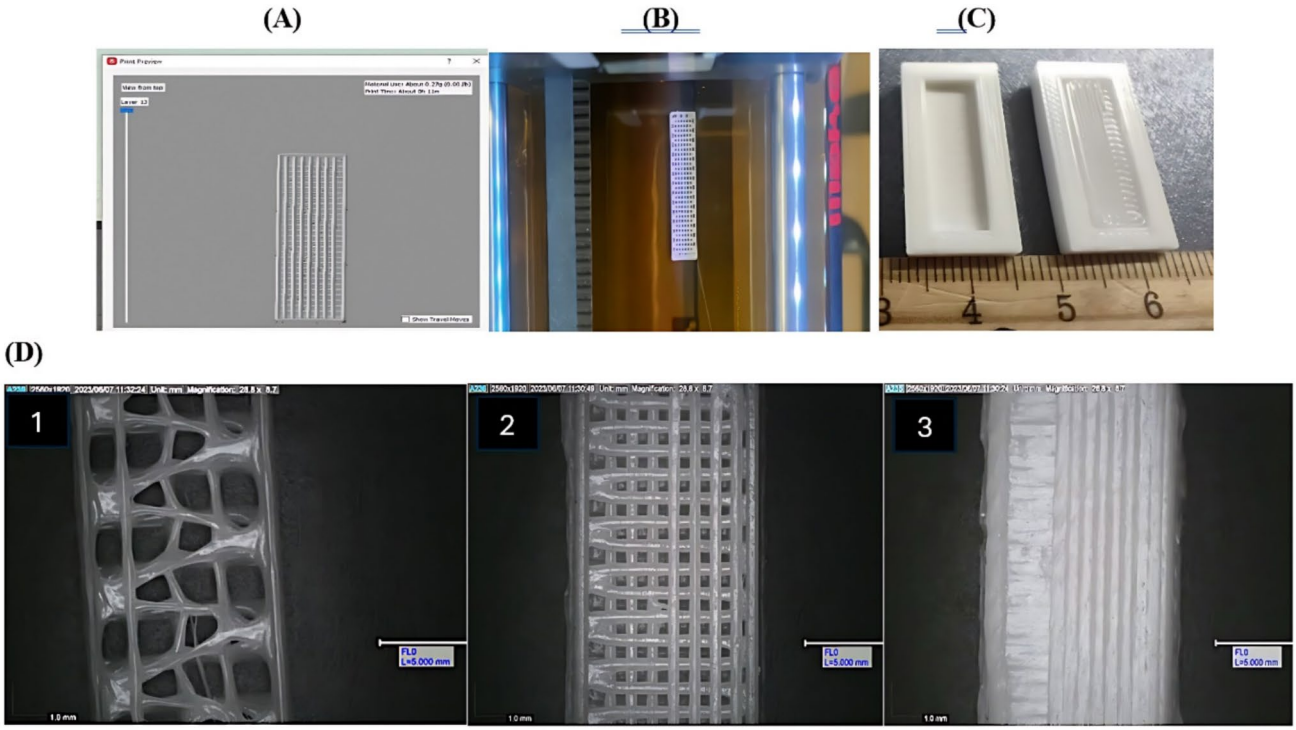

Fig. 2 **A** The implant 3D design **B** Photograph of the 3D-printed implant **C** 3D-printed PLA covers without and with the implant **D** Dino images of 20% w/w Gabapentin 3D printed implants with 1) 25% infill density 2) 50% infill density 3) 100% infill density

Japan) with a Cu Kα X-ray source (λ = 1.5418 Å). Samples were loaded into magnetic cells and placed in the XRPD instrument. Scanning covered a 2θ range of 10–30° with a 0.04° step size and 2°/min speed. Measurements used 15 mA current and 40 kV voltage. Data was plotted as 2θ *vs*. intensity for analysis [41].

3. Fourier Transform Infrared (FTIR) Spectroscopic Analysis

A Nicolet FT-IR spectrometer (Thermo Fisher Scientific, Waltham, MA) was employed for the analysis. A few milligrams of the sample were carefully placed on the sample holder, and the percentage transmittance was recorded over a spectral range of 4000–700 cm^{-1}, with a resolution of 4 cm^{-1} (averaged over 64 scans). The collected data were then processed and analyzed using Omnic™ software [41].

Morphology Characterization

1. Optical Microscopy Images:

The general structure of the 3D-printed implants was recorded with Dino-Lite™ and analyzed using the Dino Capture software.

2. Scanning Electron Microscope (SEM)

Scanning Electron Microscope (Quanta 650 FEG SEM, FEI Company, Hillsboro, OR USA) was employed to examine the surface and cross-section of the prepared filaments and printed implants. Before observation under the SEM, the samples were initially coated with a thin layer of gold using vacuum sputtering achieved with an EM Sputter Coater (EMS Sputter Coater, Hatfield, PA, USA). An accelerated voltage of 10 kV was used to capture the image [42, 43].

Energy Dispersive- x-ray (EDX) Spectroscopy

To further investigate the elemental distribution, particularly the presence of nitrogen atom (N) within the prepared filaments and implants, Energy-Dispersive X-ray analysis (EDX) was employed. The SEM used was equipped with embedded EDX capability, enabling the collection of EDX spectra to measure the elemental composition of the samples [41].

Texture Analysis

Repka-Zhang test was used to conduct 3-point bending experiments for assessing the flexibility of the filaments [44]. A TA-XT2 analyzer (Texture Technologies, Hamilton, MA, USA) equipped with the HDP/3PB probe set was employed. Filament samples were prepared as 6 cm rods and positioned on the sample holder with a 25 mm width gap. The blades were adjusted to operate at a speed of 10 mm/s until they reached a position 20 mm below the tested sample. The test was repeated ten times. PLA commercial filament was the reference material for assessing differences between standard commercial filaments and those produced through extrusion.

In Vitro Release Study

A series of *In vitro* release studies were conducted to optimize the performance of 3D-printed implants by customizing design parameters and gaining a deeper understanding of the key factors influencing drug release profiles. Specifically, we examined the effects of infill density, drug loading (expressed as the drug-to-polymer ratio), and the surface area of the implant on drug release characteristics. These parameters were systematically varied to evaluate their individual and combined impacts on the release behavior.

Prepared filaments, MeltPrep discs, and 3D-printed implants were immersed in 20 mL of phosphate-buffered saline (PBS, pH 7.4) [45]. The soaking was performed in a temperature-controlled incubator set at 37°C, with continuous agitation at 100 rpm. At predetermined time intervals, 1 mL samples were manually withdrawn and immediately replaced with an equal volume of fresh buffer to maintain sink conditions. All *In vitro* release experiments were conducted in triplicate (n = 3) to ensure reproducibility and reliability of the results.

Although a saturation solubility study was not formally conducted, Gabapentin's high aqueous solubility is well established. To confirm this experimentally, 0.5 g of Gabapentin was completely soluble in 5 mL PBS at both room temperature and 37°C, corresponding to a solubility of approximately 100 mg/mL. This ensured that sink conditions were consistently maintained throughout the *in vitro* release studies. These findings are consistent with literature data reporting Gabapentin solubility exceeding 100 mg/mL [6].

To further investigate the influence of surface area on the sustained release of gabapentin from the 3D-printed implants, a cover was fabricated using commercially available PLA filaments, featuring an opening on one side (Fig. 2). Implants with 100% infill density were inserted into this cover to assess their drug release performance under modified surface exposure conditions.

Results and Discussion

Solid State Characterization

DSC was utilized to examine the thermal properties and solid-state features of 3D-printed implants and their

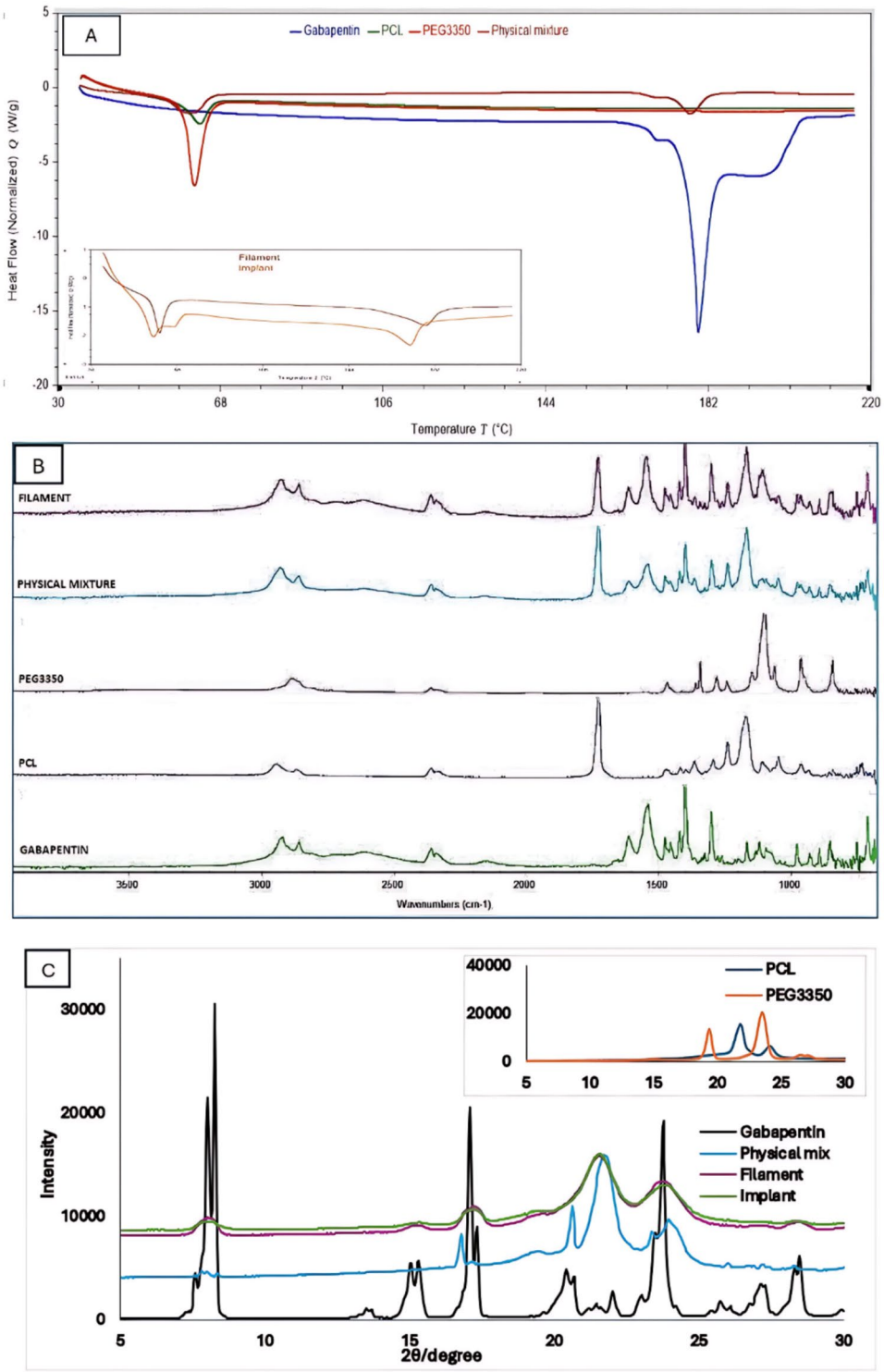

Fig. 3 Solid State Characterization study **a** DSC thermogram of Gabapentin, PCL, PEG3350, their physical mixture, loaded filaments, and implants **b** FT-IR spectra of Gabapentin, PCL, PEG3350, their physical mixture, and loaded filaments **c** XRD diffractograms of Gabapentin, PCL, PEG3350, their physical mixture, loaded filaments, and implants. * In all figures, physical mixture, filaments, and 3D printed implants contain 20% drug loading (F2 formulation)

constituent materials. The DSC thermograms, as depicted in Fig. 3, provide a comparative analysis between the Gabapentin implants and their components. The thermograph of pure Gabapentin exhibited two distinct endothermic peaks. The first peak, observed at 179.59°C, corresponds to the melting of Gabapentin, with a heat of fusion measured at 49.92 kJ/mol. The second peak, occurring at 196°C, is attributed to the thermal decomposition and subsequent loss of the drug [46]. The PCL and PEG 3350 thermograms exhibited well-defined endothermic peaks at temperatures of 58.66°C, and 59.55°C, respectively [16]. These peaks denote the crystalline melting transitions of GBP, PCL, and PEG 3350.

The DSC curve of the physical mixture showed the endothermic peak characteristic of Gabapentin but with a smaller area, reflecting the proportion of each component in the mixture. The melting points of gabapentin in the filament and implant were observed to shift to lower temperatures, specifically 177°C and 172°C, respectively. This phenomenon, known as melting point depression, occurs because the presence of the polymer (PCL) reduces the thermodynamic activity of gabapentin. The drug's molecules are more dispersed and less ordered within the polymer matrix, which lowers the energy required for the transition from a solid to a liquid state. Consequently, the chemical potential of gabapentin in the amorphous drug-polymer mixture becomes equivalent to that of the crystalline drug at a temperature lower than the pure drug's melting point. These interactions between Gabapentin and the polymer disrupt the crystalline structure, facilitating a reduced melting point [47].

To assess the residual crystallinity of Gabapentin in the formulated implants compared to the pure Gabapentin used in our study, we measured the enthalpy of melting of Gabapentin in the implants by integrating the endothermic curve, which yielded a value of approximately 44.216 J/g. The crystallinity of Gabapentin in the implants was then calculated by comparing the melting enthalpy of pure Gabapentin with that of Gabapentin in the formulation, considering the weight fraction of Gabapentin in the formulation. This analysis revealed that the residual crystallinity of Gabapentin in the formulated system was reduced to 75.84% relative to the pure Gabapentin sample used in this study [48].

The XRPD results are shown in Fig. 3. The X-ray diffraction pattern of Gabapentin confirms its crystalline nature, showing distinct peaks at 2θ values of 7.8, 13.3, 15.0, 17.0, 20.4, 21.3, 23.1, 23.6, 25.7, 27.0, and 28.2° [37]. The diffraction pattern of PCL demonstrates its semi-crystalline nature, with distinct peaks observed at 2θ angles of 21.9 and 24.2°, indicating its crystalline structure [49]. For PEG 3350, the diffractogram shows distinct peaks at 19.25° and 23.40° [50]. The diffractograms obtained from the physical mixing state, filament state, and implant state showed that the characteristic peaks of Gabapentin remained detectable at their original positions, despite being diluted with excipients, indicating the presence of residual crystallinity in the formulated implants as confirmed by the DSC data.

The FT-IR analysis was employed to analyze the chemical interactions among the components of the Gabapentin implant. Figure 3 shows the FT-IR curves of Gabapentin, PEG 3350, PCL, their physical mixtures, and the prepared filaments. Gabapentin in its solid state forms a zwitterion, which means it doesn't show the usual infrared peak for – NH stretching (3500–3300 cm – 1). Instead, it absorbs in the 3100–2800 cm – 1 range due to the – NH3 stretching vibration. The peaks within the 2300–2400 cm – 1 range are associated with the unique stretching vibration of the side chain and/or CN group. Between 1700 and 1500 cm – 1, the IR bands may be attributed to the ionized asymmetric carboxylate and NH3 deformation vibration, respectively. The IR bands between 1500 and 1350 cm – 1 were linked to the asymmetric carboxylate band and/or CH2 deformation band [51]. PCL typically demonstrates absorption peaks at distinct wavelengths, such as the stretching of asymmetric and symmetric (–CH2) bonds at 2944 cm – 1 and 2866 cm – 1, respectively. Additionally, carbonyl (C = O) stretching appears at 1702 cm – 1, while the asymmetric (C–O–C) bond stretch is observed at 1236 cm – 1 [52]. PEG 3350 exhibits characteristic peaks at 2970 and 2820 cm – 1, indicating the stretching of C-H bonds; and 1050–1000 cm – 1, linked to the C-O stretching of the alcohol [51]. The spectra from both the physical mixture and the filament state indicated that characteristic peaks of the components remained in their usual positions, suggesting that there was likely no chemical interaction between Gabapentin and any of the forming constituents.

Morphology Characterization

Optical Microscopy Images

The images captured by the DINO camera of three different implants with varying infill percentages (25%, 50%, and 100%) reveal the distinct structural characteristics of each implant. Figure 2 demonstrates the variations in infill densities of the printed implants. The implants with a 25% and 50% infill density exhibit noticeable openings throughout the structure, enhancing the available surface area in contact with the release media, which leads to faster dissolution rates. Conversely, the 100% infill density implant presents no gaps, resulting in a slower dissolution rate.

Scanning Electron Microscope

As shown in Fig. 4, SEM images of the filament illustrate a cross-sectional diameter that is in line with the die diameter (1.75 mm), indicating minimal to no enlargement during the extrusion process. The surface texture of the filament shows a smooth finish, free from visible imperfections such as cracks or roughness. This smooth surface is crucial for ensuring optimal extrusion through the 3D printer nozzle and even layer deposition during printing.

Transitioning to the implant produced by FDM with a 50% infill, the SEM images provide a detailed view of the overall structural integrity and internal infill structure. The implant shows a well-defined layer structure with consistent layer thickness, indicative of stable printing parameters. The adhesion between successive layers is another critical factor observed in the SEM images. Strong layer adhesion is

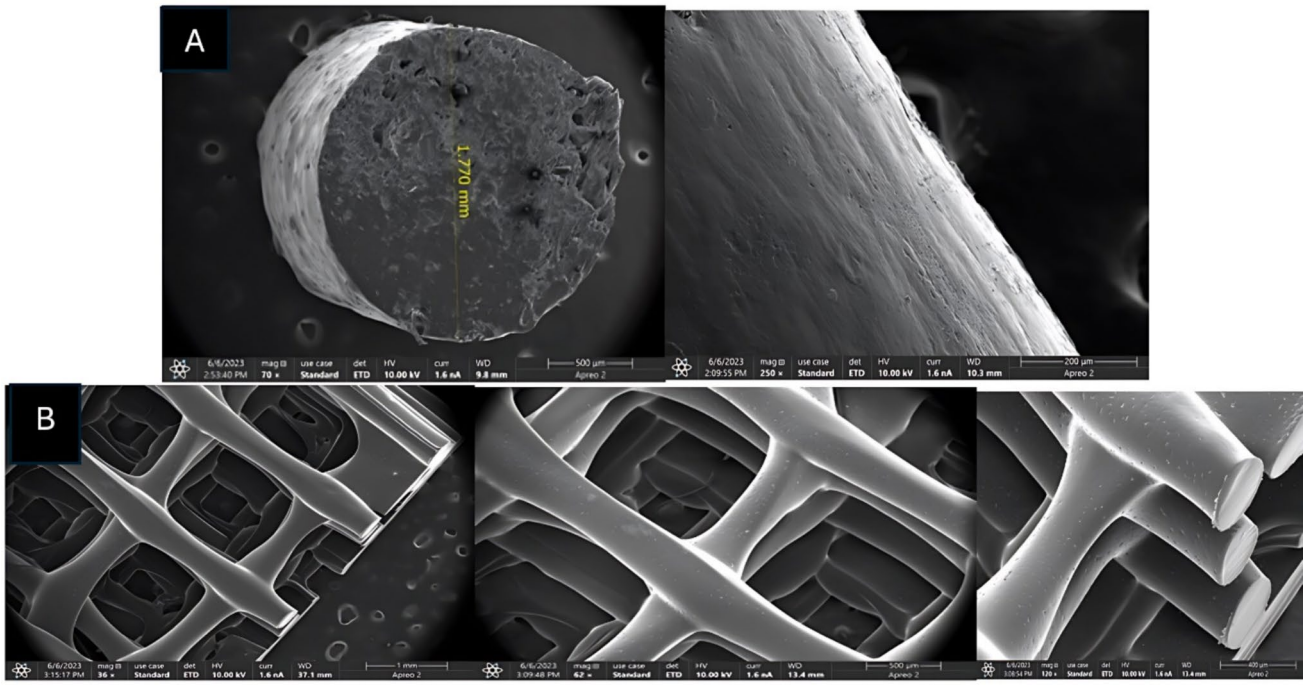

Fig. 4 SEM images of **A** extruded filaments (F2 formulation) with 1.75 mm die and **B** 3D printed implants with a detailed view of the infill structure (50% infill density)

essential for ensuring the durability and mechanical robustness of the implant. Surface features like roughness or voids can impact performance, especially in biomedical applications where smoothness influences tissue integration and biocompatibility [53].

Energy-dispersive X-ray Spectroscopy

Energy Dispersive X-ray (EDX) spectroscopy was used to examine the uniform distribution of Gabapentin within a filament. Nitrogen (N) distribution was specifically analyzed to confirm the presence and uniformity of Gabapentin, which contains nitrogen atoms, within the polymer matrix.

The EDX spectra were obtained from multiple regions across the filament cross-sections to assess the elemental distribution of nitrogen. The presence of nitrogen peaks in the EDX spectra provided a direct indication of Gabapentin distribution.

As shown in Fig. 5, the EDX maps showed a consistent distribution of nitrogen throughout the filament, suggesting that Gabapentin was uniformly distributed within the PCL-PEG matrix. Comparisons of nitrogen distribution in different sections of the filament (outer surface, mid-section, and core) revealed no significant variation This uniformity is crucial for ensuring consistent drug release profiles in potential pharmaceutical applications. Previous studies have shown similar successful uniform distribution using Hot Melt Extrusion for low-dose drugs, demonstrating the viability of this method for homogeneous drug dispersal [54, 55].

However, EDX analysis was not sufficient to differentiate the physical state of Gabapentin within the PCL matrix. While DSC and XRD confirmed that Gabapentin retains partial crystallinity, suggesting the presence of visible crystalline aggregates, the EDX mapping appeared to show a more uniform, potentially molecularly dispersed distribution. This apparent contradiction is likely due to the limited spatial resolution of the EDX technique, which may not be sensitive enough to detect micron-sized crystalline domains. To more accurately assess both the physical state and spatial distribution of Gabapentin, future studies should consider using higher-resolution techniques such as X-phase mapping.

Texture Analysis

Mechanical properties are considered one of the most important parameters for achieving good printability. The three-point bend test is a fundamental mechanical test used to evaluate the flexural properties of filaments commonly employed in 3D printing. In this test, a filament sample is placed horizontally on two support points with a defined distance between them. A load is then applied to the midpoint of the filament, causing it to bend until it fractures.

To ensure filament printability, the material must achieve an optimal balance between flexibility and brittleness. Excessive softness can cause problems such as clogging

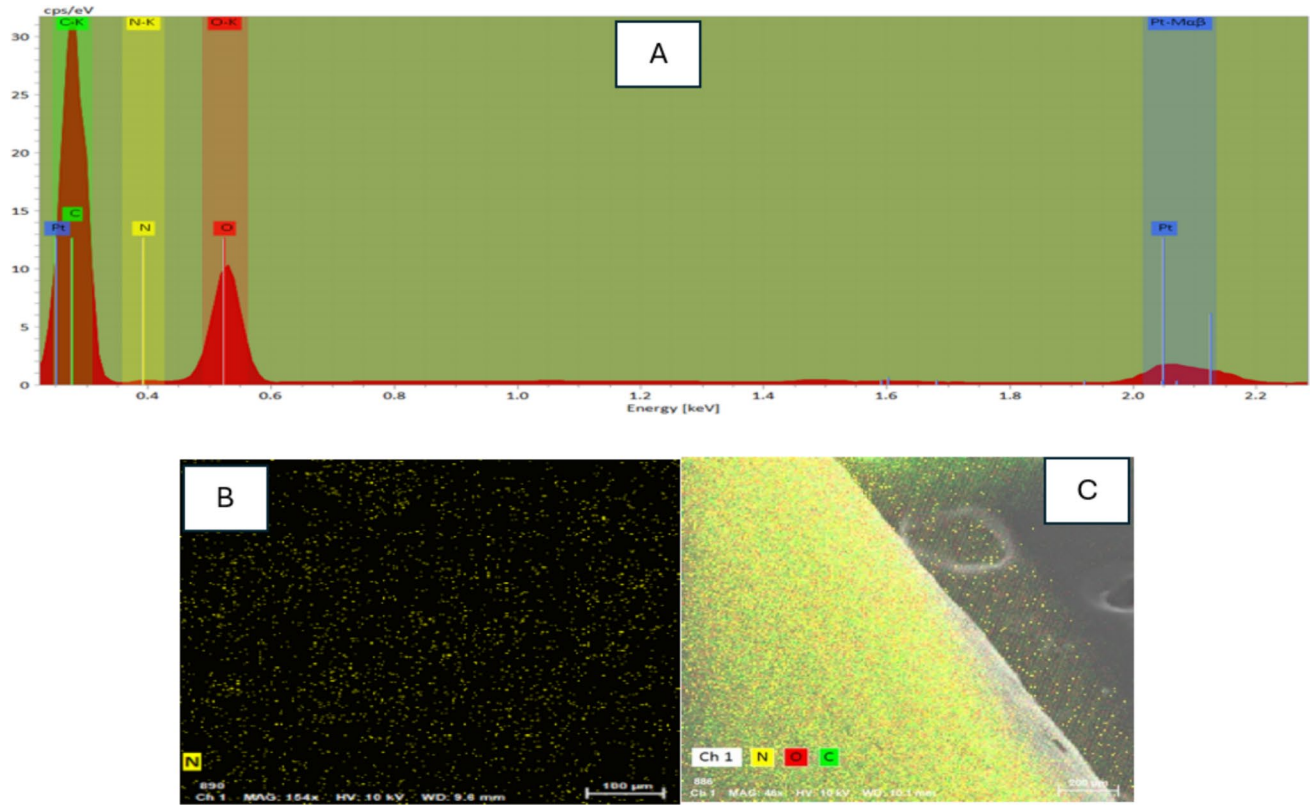

Fig. 5 EDX spectrum of the 3D-printed Gabapentin filament showing the elemental composition. Peaks corresponding to the major elements (C, O, and N) are labeled, indicating the presence of Polycaprolactone (PCL) and Gabapentin within the filament **B** EDX elemental mapping of the cross-section of a 3D-printed Gabapentin filament. The distribution of nitrogen (N) is shown, confirming the uniform dispersion of Gabapentin within the PCL matrix **C** SEM image of the surface morphology of a 3D-printed Gabapentin filament with an overlay of EDX elemental mapping. The mapping highlights the distribution of nitrogen (N) within the matrix, correlating with the presence of Gabapentin

and weak layer adhesion during printing. On the other hand, excessive brittleness can lead to frequent breakage during feeding and handling, disrupting the printing process and causing inconsistencies. Therefore, maintaining the right level of flexibility and durability is crucial for dependable and high-quality 3D printing.

The Repka-Zhang test applied in our study is designed to assess the breaking force, breaking distance, and breaking stress of a filament. In our study, the filament didn't break so we recorded the peak force. Generally, a greater breaking distance indicates better flexibility of the filaments. Stress can be calculated by dividing the force (g) over the stress area (mm^2) of the filament. Stress area can be calculated as provided by the Exponent software as $\frac{pi\left(\frac{d}{2}\right)^3}{g}$ where d is the diameter of the filament (mm) and g is the gap which represents the distance between the two supporting points (mm). In our case, it is 25 mm.

Table II shows the results of the test. PLA (1.75 mm diameter) was chosen as the reference material in our study as it is one of the most commonly available commercial materials. Incorporating the drug and PEG 3350 into the PCL polymer decreases the peak force without impacting its printability. When comparing the prepared PCL filaments to the commercial PLA filament, it was observed that the Gabapentin-loaded PCL filaments showed considerably reduced peak force and peak stress about 168.9 ± 22.7 and 2007.7 ± 269.2, respectively. This observation is in line with the results reported by Zhang *et al.*, [56] who found that filaments prepared using HPMC E5 and HPC LF, with a peak force of 243.75 and a peak stress of 2371.49, were also printable.

Table II The Repka-Zhang Test (Mean ± SD)

Filament	Peak Force (g)	Stress (g/mm^2)
20% drug loaded PCL	168.9 ± 22.7	2007.7 ± 269.2
Plain PCL	304.8 ± 36.1	3622.9 ± 408.9
Plain PLA	1440.8 ± 149.9	17124.0 ± 1781.9

In this study, the filaments remained intact throughout the process. Previous studies [57] indicate that filaments with a displacement exceeding 1.09 mm without being broken remain suitable for printing.

Release Studies

A. The Validity of Using Meltprep for Early Prediction of the Release Profile of the Implant

In the early stages of this study, our primary objective was to develop Gabapentin-loaded implants using Fused Deposition Modeling 3D printing. This required the production of drug-loaded filaments via Hot Melt Extrusion, a process that is both time-consuming and demands a substantial amount of material. Given these limitations, especially during formulation screening, we adopted melt preparation as a practical and efficient alternative for preliminary evaluation. By preparing Gabapentin-loaded discs through melt prep, initial drug release studies were conducted without the need for filament extrusion or 3D printing. This approach was used to quickly assess whether (PCL) could effectively sustain the release of Gabapentin over time. The release profiles obtained from these discs provided valuable insight into the drug's behavior within the polymer matrix and served as a predictive model for the performance of 3D-printed implants with 100% infill density. Following these preliminary results, we proceeded with HME and FDM printing of the final implant design. Notably, the release profile of the 3D-printed implants closely mirrored that of the melt-prepared discs, confirming that melt prep was a reliable tool for early-stage screening. This strategy helped us conserve materials, reduce development time, and ensure drug-polymer compatibility before committing to full-scale filament production.

The 100% infill implant (20% drug loaded) was compared to the 20% drug-loaded melt prep discs. As shown in Fig. 6A, in the initial release phase (0–5 days), the 100% infill implant demonstrated a rapid release, reaching about 30% by day 5. Similarly, the 20% Meltprep disc showed a comparable initial release, slightly lagging behind the 100% infill implant, reaching around 28% by day 5. This indicates that both formulations have a significant burst release, likely due to the high concentration of Gabapentin near the surface of the polymer matrices.

During the mid-term release phase (5–15 days), both profiles exhibited a steady release rate. The 100% infill implant achieved approximately 35% release by day 10, while the Meltprep sample reached about 33% in the same period. In the long-term release phase (15–30 days), the release from the 100% infill implant stabilized at around 40–42% by day 25. The Meltprep disc followed a closely matching release profile, stabilizing at approximately 38–40% by day 25. This long-term stability further supports the potential of the Meltprep technique to predict the release characteristics of the final 3D-printed product.

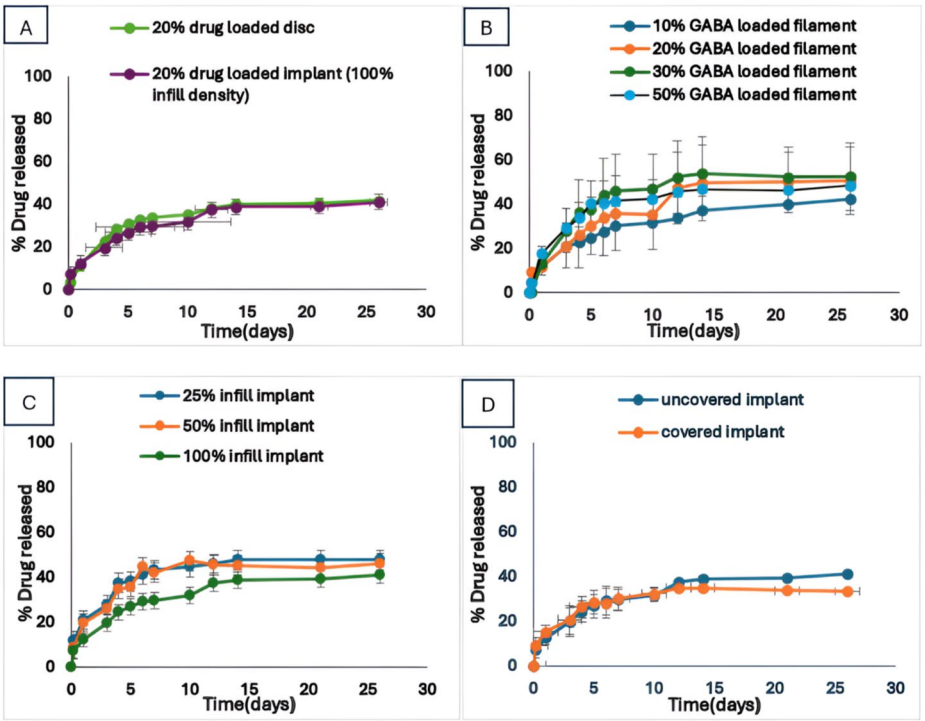

Fig. 6 Drug release study **A** Comparison of the release profiles of 3D printed 20% w/w Gabapentin implants with 100% infill density *vs* disc with the same composition prepared using Vacuum Compression Modeling **B** Release profiles from hot-melt extruded filaments with different Gabapentin loadings **C** Release profile from 3D printed Gabapentin implants (20% drug loaded) with different infill densities **D** Effect of surface area on Gabapentin release from 3D printed implants with and without cover (`n = 3)

To quantitatively compare the similarity between the two dissolution profiles, the similarity factor f_2 is used. The similarity factor f_2 is defined by the equation:

$$f_2 = 50 \times log\left(\left\{ 1 + \frac{1}{n} \sum_{t=1}^{n} \left(R_t - T_t \right)^2 \right\}^{-0.5} \times 100 \right)$$

where Rt and Tt indicate the cumulative percentage of drug released at each time point for the reference product (100% infill implant) and the test product (Meltprep disc), respectively, with n representing the total number of time points. If the f2 value is between 50 and 100, the two profiles are considered similar [58]. f2 was found to be equal to 66.8 indicating the similarity between the two dissolution profiles.

B. Effect of Drug Loading on the Release Profile

This study examines the impact of varying drug loadings on release rates, a crucial factor in optimizing implant performance. The release data revealed distinct patterns influenced by drug loading, highlighting the need to balance initial burst release with sustained drug delivery. Drug content values were determined through theoretical calculations based on formulation composition and weight, as experimental analysis was not conducted in this study [59, 60].

Filaments with different drug loadings were manufactured, and *In vitro* release data was collected. As shown in Fig. 6B, During the initial phase, rapid drug release was observed across all formulations, primarily due to the dissolution of surface-associated drug. Higher drug-loaded filaments (30% and 50%) exhibited faster initial release rates, driven by steeper concentration gradients that enhance diffusion. The 50% filament showed the most pronounced burst, releasing approximately 40% of its drug content by Day 5, followed by the 30% filament at ~ 35%. In contrast, the 20% and 10% filaments released about 30% and 20%, respectively, over the same period. These results suggest that higher drug loadings increase the availability of the drug at or near the surface, accelerating early release.

Between Days 5 and 15, the 30% and 50% filaments maintained steady release rates, reaching approximately 50–55% cumulative release. Interestingly, although the 50% filament had a higher total drug content, its release rate began to slow compared to the 30% and 20% formulations. This behavior is likely due to the physical state of the drug within the polymer matrix. At lower loadings, a high % of Gabapentin is more likely to be molecularly dispersed, promoting faster diffusion. In contrast, higher loadings may exceed the solubility limit of PCL, resulting in undissolved drug crystals that dissolve more slowly. This explanation aligns with findings reported by Holländer *et al.* [61].

Among the tested formulations, the 20% gabapentin-loaded filament emerged as a promising candidate. It achieved approximately 35% drug release by Day 5, indicating sufficient initial availability for therapeutic action, and reached a cumulative release of around 50% by Day 28, supporting a sustained release profile. This balance between an effective initial burst and prolonged delivery makes it well-suited for applications requiring both immediate and extended drug availability.

C. Effect of Infill Densities of the Implant on the Release Profile

Figure 6C shows that adjusting the infill density is a useful way to control drug release from the manufactured implants. Lowering the infill density from 100 to 50% and 25% increases internal porosity and surface area, which enhances water penetration and accelerates drug release. Within the first 10 days, the 100% infill implants released about 30% of the drug, compared to approximately 46% released by the 25% and 50% infill implants over the same period.

Interestingly, the 25% and 50% infill implants showed a very similar release behavior, and a similarity factor (f_2) value of 78.7 confirmed that their overall release profiles were statistically equivalent. These findings suggest that varying the infill density between 25 and 50% does not significantly impact the drug release kinetics, as both designs exhibit statistically similar release profiles. However, increasing the infill to 100% results in a noticeably slower and more sustained release, likely due to the reduced porosity and longer diffusion path. This highlights the potential of using infill density as a design parameter to tailor release rates, with 25% and 50% infill suitable for moderate release needs, and 100% infill better suited for applications requiring prolonged drug delivery, making it more appropriate for applications requiring prolonged drug delivery.

To better understand the kinetics of drug release, we examined the *In vitro* drug release profiles using several mathematical models. We evaluated how well these models fit the data by calculating the coefficient of determination (r^2) and used the release exponent to gain insights into the drug release mechanism [61].

As seen in Table III, the Korsmeyer-Peppas model appears to best fit the release profiles of Gabapentin from the PCL filaments and implants, as indicated by the highest r^2 values. This suggests that the drug release is governed by a diffusion-controlled process. Furthermore, the release exponent (n) values obtained from the Korsmeyer–Peppas model were consistently below 0.5, indicating that the release of Gabapentin followed Fickian diffusion. In this mechanism, drug molecules diffuse through the hydrated polymer matrix, and the rate of release is primarily controlled by the concentration gradient and the diffusivity of the drug within the polymer.

Table III Kinetics of Gabapentin Drug Release: Coefficient of Determination (r^2) and Release Exponent (n)

	Zero	First	Higuchi	Korsmeyer peppas	
	r^2			r^2	n
F1 Filament	0.8690	0.2067	0.9773	0.9932	0.4513
F2 Filament	0.8703	0.1573	0.9609	0.9651	0.3903
F2 implant (25% infill)	0.7361	0.2024	0.9047	0.9818	0.3129
F2 Implant (50% infill)	0.7068	0.2086	0.8830	0.9682	0.3685
F2 Implant (100% infill)	0.8427	0.2126	0.9636	0.9917	0.3778
F3 Filament	0.7713	0.1546	0.9236	0.9765	0.5523
F4 Filament	0.7402	0.1949	0.9068	0.9547	0.4997

D. Effect of Surface Area on the Release Profile

Figure 6D compares the release profiles of Gabapentin from covered and uncovered implants. The two profiles appear nearly identical, which is supported by a similarity factor (f_2) value of 72.8, indicating statistical equivalence. This suggests that the drug release from the implants is primarily governed by diffusion through the polymer matrix rather than by the surface area exposed to the release medium. Once the implant core becomes hydrated, drug diffusion proceeds through the swollen PCL matrix, and masking certain surfaces has minimal impact on the overall release behavior.

Clinical Limitations and Future Work

1. Implant Dimensions

The dimensions of the developed implant were slightly larger than those of commercially available pediatric implants, such as *Supprelin® LA*, which measures approximately 3.5 cm in length and 2 mm in diameter. However, this limitation can be readily addressed through customization using 3D printing technology, allowing for precise tailoring to patient-specific anatomical and therapeutic needs.

2. Gabapentin Loading

The gabapentin load in the implant was significantly lower than typical oral doses. This is due to the subcutaneous route of administration, which bypasses the variable gastrointestinal absorption and first-pass metabolism associated with oral delivery. As a result, the therapeutically effective dose is expected to be lower. Nevertheless, *in vivo* studies are necessary to validate the pharmacokinetics and therapeutic efficacy of the implant formulation. In cases where higher drug doses are required, the use of multiple subcutaneous implants offers a practical and scalable solution [62]. To support such applications, implant geometry can be optimized for patient comfort and drug delivery efficiency. This customization is readily achievable through 3D printing technology.

3. Drug Release Duration

The current formulation exhibits a relatively short duration of drug release, which may limit its utility for chronic conditions. Future work will focus on optimizing the release profile by exploring alternative biodegradable polymers and incorporating degradable barrier coatings. The goal is to extend the release period to at least 8 weeks, making the system more suitable for long-term therapeutic applications [63].

Conclusions

In our research, we have successfully engineered Gabapentin implants by combining Fused Deposition modeling 3D printing with Hot-Melt Extrusion. Utilizing Vacuum Compression Modeling, we accurately predicted drug release profiles and employed Hot Melt Extrusion to produce filaments with varying Gabapentin concentrations. The printability of these filaments was confirmed through the Repka-Zhang test, and they were subsequently used in FDM printing to fabricate implants with diverse infill densities. The physicochemical analysis of the 3D-printed implants revealed strong compatibility between Gabapentin and the excipients. This study underscores the efficacy of 3D printing technique in creating implants with highly customizable release profiles, offering significant advances in personalized medicine. It also enables tailored drug release and loadings to meet individual patients' needs.

Author Contributions B.A.D: conceptualization, methodology, data curing, formal analysis, and writing-original draft; H.M.A: conceptualization, methodology, data curing, formal analysis, and writing-original draft; M.M.: supervision, funding acquisition, review, and editing.

Funding The research reported herein was partly supported by Maniruzzaman's start-up funds at the University of Texas at Austin and the Egyptian Government, which financed Hala Abdelhakk's PhD program. Baher A. Daihom would like to express his gratitude to the Binational Fulbright Commission in Egypt for supporting his post-doctoral fellowship at the University of Texas at Austin.

Data Availability Data will be made available on request.

Declarations

Conflict of interest The authors declare the following conflict of interest. Mohammed Maniruzzaman (M.M.), an author of this manuscript, holds stock in, serves on a scientific advisory board for, or is a consultant for CoM3D Ltd. (Surrey, UK), DosePlus Therapeutics, Inc. (Princeton, NJ, USA), SmarGic Tech LLC (Oxford, MS, USA), and Septum Solutions LLC (Houston, TX, USA). The terms of this arrangement have been reviewed and approved by the University of Texas at Austin and the University of Mississippi (Ole Miss) in accordance with their policies on objectivity in research. The companies had no role in the design of the study; in the collection, analyses, or interpretation of data; in the writing of the manuscript; and in the decision to publish the results.

References

1. Walker SM. Neuropathic pain in children: Steps towards improved recognition and management. EBioMedicine. 2020;1:62.
2. Colloca L, Ludman T, Bouhassira D, Baron R, Dickenson AH, Yarnitsky D, Freeman R, Truini A, Attal N, Finnerup NB, Eccleston C. Neuropathic pain. Nat Rev Dis Primers. 2017;3:1–9.
3. Dworkin RH, O'connor AB, Backonja M, Farrar JT, Finnerup NB, Jensen TS, Kalso EA, Loeser JD, Miaskowski C, Nurmikko TJ, Portenoy RK. Pharmacologic management of neuropathic pain: evidence-based recommendations. Pain. 2007;132:237–51.
4. Walco GA, Dworkin RH, Krane EJ, LeBel AA, Treede RD. Neuropathic pain in children: special considerations. In: Mayo Clinic Proceedings. Vol. 85, (No. 3). Elsevier; 2010. pp. S33–S41.
5. Bartelink IH, Rademaker CM, Schobben AF, Van Den Anker JN. Guidelines on paediatric dosing on the basis of developmental physiology and pharmacokinetic considerations. Clin Pharmacokinet. 2006;45:1077–97.
6. Bockbrader HN, Wesche D, Miller R, Chapel S, Janiczek N, Burger P. A comparison of the pharmacokinetics and pharmacodynamics of pregabalin and gabapentin. Clin Pharmacokinet. 2010;49:661–9.
7. Meaadi J, Obara I, Eldabe S, Nazar H. The safety and efficacy of gabapentinoids in the management of neuropathic pain: a systematic review with meta-analysis of randomised controlled trials. Int J Clin Pharm. 2023;45:556–65.
8. Goodman CW, Brett AS. A clinical overview of off-label use of gabapentinoid drugs. JAMA Intern Med. 2019;179:695–701.
9. Chen O, Cadwell JB, Matsoukas K, Hagen J, Afonso AM. Perioperative gabapentin usage in pediatric patients: A scoping review. Paediatr Anaesth. 2023;33:598–608.
10. Bannister K, Qu C, Navratilova E, Oyarzo J, Xie JY, King T, et al. Multiple sites and actions of gabapentin-induced relief of ongoing experimental neuropathic pain. Pain. 2017;158:2386–95.
11. Buck ML. Gabapentin use in postoperative and neuropathic pain in children. Pediatr Pharmacother. 2016;22.
12. Kaul I, Amin A, Rosenberg M, Rosenberg L, Meyer WJ. Use of gabapentin and pregabalin for pruritus and neuropathic pain associated with major burn injury: a retrospective chart review. Burns. 2018;44:414–22.
13. Moore RA, Wiffen PJ, Derry S, Rice AS. Gabapentin for chronic neuropathic pain and fibromyalgia in adults. In: Cochrane database of systematic reviews. 2014.
14. Trudeau V, Myers S, LaMoreaux L, Anhut H, Garofalo E, Ebersole J. Gabapentin in naive childhood absence epilepsy: results from two double-blind, placebo-controlled, multicenter studies. J Child Neurol. 1996;11:470–5.
15. Dougherty JA, Rhoney DH. Gabapentin: a unique anti-epileptic agent. Neurol Res. 2001;23:821–9.
16. Carcaboso ÁM, Chiappetta DA, Höcht C, Blake MG, Boccia MM, Baratti CM, et al. In vitro/in vivo characterization of melt-molded gabapentin-loaded poly(epsilon-caprolactone) implants for sustained release in animal studies. Eur J Pharm Biopharm. 2008;70:666–73.
17. Blake MG, Boccia MM, Carcaboso ÁM, Chiappetta DA, Höcht C, Krawczyk MC, et al. Novel long-term anticonvulsant treatment with gabapentin without causing memory impairment in mice. Epilepsy Behav. 2010;17:157–64.
18. Chaudhari VS, Kushram P, Bose S. Drug delivery strategies through 3D-printed calcium phosphate. Trends Biotechnol. 2024;42:1396–409.
19. Kutlehria S, D'Souza A, Bleier BS, Amiji MM. Role of 3D printing in the development of biodegradable implants for central nervous system drug delivery. Mol Pharm. 2022;19:4411–27.
20. Liu G, He Y, Liu P, Chen Z, Chen X, Wan L, Li Y, Lu J. Development of bioimplants with 2D, 3D, and 4D additive manufacturing materials. Engineering. 2020;;6:1232–43.
21. Holkunde A, Karnik I, Uttreja P, Narala N, Wang H, Elkanayati RM, Vemula SK, Repka MA. Personalized medicine through semi-isolid-extrusion based 3D printing: Dual-drug loaded gummies for enhanced patient compliance. Pharm Res. 2025;42:185–201.
22. Goyanes A, Robles Martinez P, Buanz A, Basit AW, Gaisford S. Effect of geometry on drug release from 3D printed tablets. Int J Pharm. 2015;494:657–63.
23. Vaz VM, Kumar L. 3D printing as a promising tool in personalized medicine. Aaps Pharmscitech. 2021;22:49.
24. Goole J, Amighi K. 3D printing in pharmaceutics: A new tool for designing customized drug delivery systems. Int J Pharm. 2016;499:376–94.
25. Goyanes A, Chang H, Sedough D, Hatton GB, Wang J, Buanz A, et al. Fabrication of controlled-release budesonide tablets via desktop (FDM) 3D printing. Int J Pharm. 2015;496:414–20.
26. Iqbal H, Fernandes Q, Idoudi S, Basineni R, Billa N. Status of polymer fused deposition modeling (FDM)-based three-dimensional printing (3DP) in the pharmaceutical industry. Polymers. 2024;16:386.
27. Ahmed W, Alnajjar F, Zaneldin E, Al-Marzouqi AH, Gochoo M, Khalid S. Implementing FDM 3D printing strategies using natural fibers to produce biomass composite. Materials. 2020;13:4065.
28. Kempin W, Franz C, Koster LC, Schneider F, Bogdahn M, Weitschies W, et al. Assessment of different polymers and drug loads for fused deposition modeling of drug loaded implants. Eur J Pharm Biopharm. 2017;115:84–93.
29. Peng H, Han B, Tong T, Jin X, Peng Y, Guo M, Li B, Ding J, Kong Q, Wang Q. 3D printing processes in precise drug delivery for personalized medicine. Biofabrication. 2024;16:032001.
30. Li X, Hong X, Shuai S, Han X, Li C, Zhang H, Wang Z, Ren M, Jin L, Zheng A. A review of hot melt extrusion technology: advantages, applications, key factors and future prospects. J Drug Deliv Sci Technol. 2024;98:105884.
31. Shadambikar G, Kipping T, Di-Gallo N, Elia AG, Knüttel AN, Treffer D, et al. Vacuum compression molding as a screening tool

to investigate carrier suitability for hot-melt extrusion formulations. Pharmaceutics. 2020;12:1–17.
32. Eder S, Beretta M, Witschnigg A, Koutsamanis I, Eggenreich K, Khinast JG, et al. Establishment of a molding procedure to facilitate formulation development for co-extrudates. AAPS PharmSciTech. 2017;18:2971–6.
33. Mueller V, Caldas BS, Radovanovic E, Muniz EC. Development of hot melt extruded polycaprolactone (PCL) matrices for an oral ultra-long-lasting delivery of galantamine for Alzheimer's disease therapy. J Drug Deliv Sci Technol. 2025;104:106464.
34. Khandan A, Esmaeili S. Fabrication of polycaprolactone and polylactic acid shapeless scaffolds via fused deposition modelling technology. J Adv Mater Process. 2019;7:16–29.
35. Mohammed MR. Mechanical and biological behaviour of 3D printed PCL-based scaffolds fabricated by fused deposition modelling for bone tissue engineering: a review of recent advances. Misan J Eng Sci. 2022;1:33–46.
36. Silverman LA, Neely EK, Kletter GB, Lewis K, Chitra S, Terleckyj O, et al. Long-term continuous suppression with once-yearly histrelin subcutaneous implants for the treatment of central precocious puberty: a final report of a phase 3 multicenter trial. J Clin Endocrinol Metab. 2015;100:2354–63.
37. Rimawi IB, Muqedi RH, Kanaze FI. Development of gabapentin expandable gastroretentive controlled drug delivery system. Sci Rep. 2019;9:11675.
38. Dauer K, Wagner KG. Micro-Scale Vacuum Compression Molding as a Predictive Screening Tool of Protein Integrity for Potential Hot-Melt Extrusion Processes. Pharmaceutics. 2023;15:723.
39. Bandari S, Nyavanandi D, Dumpa N, Repka MA. Coupling hot melt extrusion and fused deposition modeling: Critical properties for successful performance. Adv Drug Deliv Rev. 2021;172:52–63.
40. Nashed N, Lam M, Nokhodchi A. A comprehensive overview of extended release oral dosage forms manufactured through hot melt extrusion and its combination with 3D printing. Int J Pharm. 2021;596:120237.
41. Lu A, Duggal I, Daihom BA, Zhang Y, Maniruzzaman M. Unraveling the influence of solvent composition on Drop-on-Demand binder jet 3D printed tablets containing calcium sulfate hemihydrate. Int J Pharm. 2024;649:123652.
42. Fayez H, Daihom B, Abd El-Aleem Y, Ibrahim IT, Motaleb MA. Brain nanotargeted [131I] I-Rolapitant as a model for brain imaging: intranasal formulation, radiolabelling, biodistribution, and comparative study. J Drug Deliv Sci Technol. 2023;86:104705.
43. Wassif RK, Daihom BA, Maniruzzaman M. FRESH 3D printing of zoledronic acid-loaded chitosan/alginate/hydroxyapatite composite thermosensitive hydrogel for promoting bone regeneration. Int J Pharm. 2024;667:124898.
44. Wang H, Dumpa N, Bandari S, Durig T, Repka MA. Fabrication of taste-masked donut-shaped tablets via fused filament fabrication 3D printing paired with hot-melt extrusion techniques. AAPS PharmSciTech. 2020;21:243.
45. Ramchandani M, Robinson D. In vitro and in vivo release of ciprofloxacin from PLGA 50: 50 implants. J Control Release. 1998;54:167–75.
46. Hsu CH, Lin SY. Rapid examination of the kinetic process of intramolecular lactamization of gabapentin using DSC-FTIR. Thermochim Acta. 2009;486:5–10.
47. Marsac PJ, Li T, Taylor LS. Estimation of drug-polymer miscibility and solubility in amorphous solid dispersions using experimentally determined interaction parameters. Pharm Res. 2009;26:139–51.
48. Pan X, Julian T, Augsburger L. Quantitative measurement of indomethacin crystallinity in indomethacin-silica gel binary system using differential scanning calorimetry and X-ray powder diffractometry. Aaps Pharmscitech. 2006;7:11.
49. Balu R, Sampath Kumar TS, Ramalingam M, Ramakrishna S. Electrospun polycaprolactone/Poly(1,4-butylene adipate-co-polycaprolactam) blends: potential biodegradable scaffold for bone tissue regeneration. J Biomater Tissue Eng. 2011;1:30–9.
50. Barron MK, Young TJ, Johnston KP, Williams RO. Investigation of processing parameters of spray freezing into liquid to prepare polyethylene glycol polymeric particles for drug delivery. Aaps Pharmscitech. 2003;4:12.
51. Sahu M, Reddy VR, Kim B, Patro B, Park C, Kim WK, Sharma P. Fabrication of Cu2ZnSnS4 light absorber using a cost-effective mechanochemical method for photovoltaic applications. Materials. 2022;15:1708.
52. Benkaddour A, Jradi K, Robert S, Daneault C. Grafting of polycaprolactone on oxidized nanocelluloses by click chemistry. Nanomaterials. 2013;3:141–57.
53. Thumsorn S, Prasong W, Kurose T, Ishigami A, Kobayashi Y, Ito H. Rheological behavior and dynamic mechanical properties for interpretation of layer adhesion in FDM 3D printing. Polymers. 2022;14:2721.
54. Scoutaris N, Vithani K, Slipper I, Chowdhry B, Douroumis D. SEM/EDX and confocal raman microscopy as complementary tools for the characterization of pharmaceutical tablets. Int J Pharm. 2014;470:88–98.
55. Park JB, Kang CY, Kang WS, Choi HG, Han HK, Lee BJ. New investigation of distribution imaging and content uniformity of very low dose drugs using hot-melt extrusion method. Int J Pharm. 2013;458:245–53.
56. Zhang J, Feng X, Patil H, Tiwari RV, Repka MA. Coupling 3d printing with hot-melt extrusion to produce controlled-release tablets. Int J Pharm. 2017;519:186–97.
57. Đuranović M, Obeid S, Madžarević M, Cvijić S, Ibrić S. Paracetamol extended release FDM 3D printlets: Evaluation of formulation variables on printability and drug release. Int J Pharm. 2021;592:120053.
58. Costa P, Lobo JM. Modeling and comparison of dissolution profiles. Eur J Pharm Sci. 2001;13:123–33.
59. Liaskoni A, Wildman RD, Roberts CJ. 3D printed polymeric drug-eluting implants. Int J Pharm. 2021;597:120330.
60. Yang Y, Wu H, Fu Q, Xie X, Song Y, Xu M, Li J. 3D-printed polycaprolactone-chitosan based drug delivery implants for personalized administration. Mater Des. 2022;214:110394.
61. Mhlanga N, Ray SS. Kinetic models for the release of the anticancer drug doxorubicin from biodegradable polylactide/metal oxide-based hybrids. Int J Biol Macromol. 2015;72:1301–7.
62. Shoupe D, Mishell DR. Norplant: subdermal implant system for long-term contraception. Am J Obstet Gynecol. 1989;160:1286–92.
63. Basak P, Adhikari B, Banerjee I, Maiti TK. Sustained release of antibiotic from polyurethane coated implant materials. J Mater Sci Mater Med. 2009;20:213–21.